

Spiral Defect Chaos in Large Aspect Ratio Rayleigh-Bénard Convection

Stephen W. Morris,^{*} Eberhard Bodenschatz,[†]
David S. Cannell, and Guenter Ahlers

*Department of Physics and
Center for Nonlinear Science
University of California
Santa Barbara, CA 93106-9530*

We report experiments on convection patterns in a cylindrical cell with a large aspect ratio. The fluid had a Prandtl number $\sigma \approx 1$. We observed a chaotic pattern consisting of many rotating spirals and other defects in the parameter range where theory predicts that steady straight rolls should be stable. The correlation length of the pattern decreased rapidly with increasing control parameter so that the size of a correlated area became much smaller than the area of the cell. This suggests that the chaotic behavior is intrinsic to large aspect ratio geometries.

Submitted to Phys. Rev. Lett. May 12 1993.

PACS No. 47.20.Bp

Rayleigh-Bénard convection, the instability of a horizontal fluid layer heated from below, has served as a paradigm for the study of nonlinear pattern formation in systems under nonequilibrium conditions.¹ One important reason for this is the extensive nonlinear stability analysis that has been carried out by Busse and Clever,^{2,3} which provides an unusually detailed picture of the secondary instabilities expected for this system. The onset of convection occurs when the temperature difference ΔT across the layer exceeds a critical value ΔT_c . For $\Delta T > \Delta T_c$, the quiescent layer becomes unstable to a periodic pattern of convection rolls with wavenumber k . The stability analysis showed that there is a well defined region in the $\Delta T - k$ plane, known as the "Busse balloon", within which time-independent straight rolls are predicted to be stable. The detailed size and shape of the balloon depends on the Prandtl number $\sigma = \nu/\kappa$, where ν is the kinematic viscosity and κ the thermal diffusivity.

In this Letter we report experimental results for convection in gaseous CO_2 ($\sigma \simeq 0.96$) in a large aspect ratio system ($\Gamma = \text{radius} / \text{height} = 78$). In much of the regime where theory predicts time-independent parallel straight rolls, we observed instead a spatially disorganized time-dependent state consisting of many localized rotating spirals and other defects. There were both right- and left-handed spirals which rotated clockwise and counterclockwise, respectively. Most were single armed, but we also observed two- and three- armed spirals and patches of concentric rolls. The spirals were *not* created in pairs, but rather emerged from and coexisted with surrounding highly disordered regions in the pattern. Usually, spirals were created and destroyed in the interior of the cell well away from the boundaries. The overall pattern appeared to be chaotically time-dependent. Our results indicate⁴ that this state is representative of convection in large- Γ systems with $\sigma \approx 1$. This is consistent with early observations on a large- Γ sample using liquid Helium,⁵ but in that work the patterns were not visualized.

It is well known that defects and roll curvature give rise to large scale mean flows^{6–8} which can in turn advect the rolls, leading to complex time dependence. Such flows have much more pronounced effects at low σ . We are unable to visualize such flows, but recent numerical simulations⁹ suggest that they are important for understanding the spiral-defect-chaos state.

Our convection cell consisted of a sapphire top plate and a polished aluminum bottom plate, each 0.95 cm thick. The bottom plate had a film heater glued to its lower surface. The lateral boundaries were constructed of three layers of porous filter paper which was compliant enough to allow the cell height to be adjusted by up to $10\mu m$ by means of three piezoelectric stacks. The height d was $568\mu m$, uniform to $\pm 1\mu m$. The cell height and its uniformity were measured interferometrically. The paper sidewalls produced smaller lateral temperature gradients than the solid ones used previously¹⁰ and caused the pattern to prefer a roll orientation perpendicular to them. For most of the results reported here the pressure was 32.7 ± 0.1 bar, regulated to $\pm 0.01\%$. The temperature of the upper surface of the top plate was held at $24.00\pm 0.02^\circ C$ and regulated to $\pm 2mK$ by means of circulating water maintained at the same pressure as the gas. The bottom-plate temperature was measured by means of an embedded thermistor and regulated to $\pm 0.5mK$. This temperature was varied as the experimental control parameter. This protocol caused the average temperature, and thus the average fluid properties, to vary with control parameter. We define the reduced temperature difference $\epsilon \equiv (\Delta T/\Delta T_{c0})-1$, where ΔT_{c0} is the critical temperature difference for a fluid having properties corresponding to those of a sample at the average temperature \bar{T} . We found the onset of convection at $\Delta T_c = 6.622\pm 0.005^\circ C$, and used the known temperature dependence of the gas properties to obtain $\Delta T_{c0}(\bar{T})$. The characteristic time scale is the vertical thermal diffusion time $t_v \equiv d^2/\kappa \simeq 1.3s$. t_v varied about 15% over our range

of \bar{T} , while the Prandtl number $\sigma \simeq 0.96$ varied only about 3%.¹¹ The patterns were visualized using the shadowgraph method.¹²

The states we studied were formed by increasing ϵ from just below onset to the desired final value in a short time ($\sim 10t_v$). After this quench we waited at least two horizontal diffusion times $t_h \equiv \Gamma^2 t_v \simeq 2.2h$, for transients to decay. We used this procedure as a matter of convenience only; we have obtained similar patterns by increasing ϵ slowly ($t_v \frac{d\epsilon}{dt} \simeq 10^{-5}$).

Examples of patterns observed for small ϵ are shown in Fig. 1. For $\epsilon \lesssim 0.050$ we found essentially straight rolls in agreement with theory as shown in image 1(a). The rolls showed a progressive tendency to become normal to the sidewalls with increasing ϵ , which resulted in strong curvature together with focus singularities at the sidewalls as shown in image 1(b) for $\epsilon = 0.116$. This state showed persistent time dependence on timescales of order t_h , attributable to the motion of defects, grain boundaries and foci. This behavior is reminiscent of observations made in a previous studies^{13,14} of water in cylindrical cells.

With increasing ϵ , time dependence on shorter time scales [$\mathcal{O}(100t_v)$] developed in the *interior* of the cell. It took the form of transient rotating spiral patches at $\epsilon \simeq 0.4$, and for $\epsilon \gtrsim 0.5$ a sea of interacting rotating spirals and other mobile defects existed in the interior as shown in image 2(a).^{4,15} With further increase in ϵ the area occupied by the foci on the sidewalls decreased until the cell was filled with what we have termed "spiral defect chaos", as shown in image 2(b) for $\epsilon = 0.721$. Individual spirals typically rotated several times while translating a distance comparable to their diameter before being destroyed or suffering a change in the number of arms. A common process resulting in a change in the number of arms consisted of a dislocation gliding into the spiral core. Occasionally, successive events

of this kind left a spiral with opposite handedness to the original. Spirals were generally created and destroyed by complicated processes involving interactions with the other non-spiral defects in the pattern, rather than with other spirals. The timescale for the dynamics decreased with increasing ϵ , but a detailed account of the temporal behavior is beyond the scope of this Letter.

We characterized these patterns using the structure function $S(\vec{k})$, equal to the time average of the square of the modulus of the spatial Fourier transform of the shadowgraph signal. $S(\vec{k})$ provides quantitative information regarding the spatial scales of the roll patches. We prefiltered the images by multiplying them by a radial Hanning function $H(r) \equiv [1 + \cos(\pi r/r_0)]/2$ for $r \leq r_0$ and $H(r) \equiv 0$ for $r > r_0$. We used $r_0 = 0.71\Gamma$ in units of d , and averaged 256 measurements of $S(\vec{k})$ taken at intervals of order several hundred t_v . $S(\vec{k})$ progressed from a few sharp peaks to a broad ring as ϵ was increased. For $\epsilon \gtrsim 0.4$, where many spirals appear, $S(\vec{k})$ was nearly azimuthally symmetric, i.e., it depended only on $k \equiv |\vec{k}|$ and not on \vec{k} . At each ϵ , we performed an azimuthal average in \vec{k} -space to obtain better statistics for $S(k)$. A typical result is presented in Fig. 3.

In terms of the first two moments

$$\langle k \rangle \equiv \frac{\int |\vec{k}| S(\vec{k}) d^2 \vec{k}}{\int S(\vec{k}) d^2 \vec{k}} = \frac{\int_0^\infty k^2 S(k) dk}{\int_0^\infty k S(k) dk} \quad (1)$$

and

$$\langle k^2 \rangle \equiv \frac{\int |\vec{k}|^2 S(\vec{k}) d^2 \vec{k}}{\int S(\vec{k}) d^2 \vec{k}} = \frac{\int_0^\infty k^3 S(k) dk}{\int_0^\infty k S(k) dk} \quad (2)$$

of $S(\vec{k})$, we define an average wavevector $\langle k \rangle$ and a correlation length

$$\xi \equiv [\langle k^2 \rangle - \langle k \rangle^2]^{-1/2}. \quad (3)$$

Our results for $\xi(\epsilon)$ in units of d are presented in Fig. 4. The solid line is a fit to a power law of the form $\xi = \xi_0 \epsilon^{-\nu}$, and yields $\xi_0 = (2.4 \pm 0.1)d$ and $\nu = 0.43 \pm 0.05$. Obviously,

ξ decreases strongly with increasing ϵ , and is only of order a few d for $\epsilon \gtrsim 1$. Under these conditions a correlation area ($\pi\xi^2$) occupies less than 0.1% of the total cell area. A statistical description in the infinite- Γ limit¹ might accurately characterize our experiments for $\epsilon \gtrsim 1$. We also show ξ for runs at two other pressures which span a range of fluid parameters.¹¹ We find very similar behavior in these cases, with ξ tending to increase slightly with pressure, for fixed ϵ .

The mean wavevector $\langle k \rangle$ of the pattern decreased with increasing ϵ in such a way that it stayed well within the theoretically stable region^{3,16} (the Busse balloon) as shown in Fig. 5. It has previously been suggested that pattern instabilities,¹⁷ or the onset of complex time dependence,^{8,14,18} occur when the wavevector distortion required to meet the lateral boundary conditions forces the pattern to become unstable by *locally* exceeding the stability limits of the uniform infinite pattern. The analog of this cell geometry dominated situation in our cell would seem to be the slowly time dependent state we observed for $\epsilon \lesssim 0.2$. On the other hand, the nucleation and proliferation of spiral defects observed at higher ϵ does not fit this picture. The chaotic state is already well developed when only a small fraction of the wavevector distribution lies outside the Busse balloon as shown in Fig. 3. It seems more reasonable to explain the broadening of the wavevector distribution as a consequence of the disordering effects of dynamics intrinsic to the pattern, rather than as a response to boundary conditions. At higher ϵ , the wavevector distribution extends over both boundaries of the Busse balloon, and we do occasionally observe, for example, the nucleation of a pair of dislocations in places where rolls are pushed close together.

The rotation of the spiral defects is a particularly striking feature of the chaotic state. Periodic states involving dislocations and spirals, both rotating¹⁰ and nonrotating,⁸ have

been observed previously in gas convection, but in these cases the spirals spanned the experimental cell and were influenced by special lateral boundary conditions. In our experiments, it is clear that the spirals are coherent structures¹ which emerge as part of the chaotic dynamics, and are unrelated to the lateral boundaries. Our results naturally raise the question of why the experimental patterns differ so dramatically from the theoretical expectations. It appears that the straight-roll state is a rather special situation;¹⁹ the attractor basin of straight rolls apparently does not overlap with the initial conditions and boundary conditions accessible to the experiment. The spiral defect chaos found at $\epsilon \gtrsim 1$ is no longer dominated by the boundaries, and presumably represents a different, unsteady state that would persist in the infinite- Γ limit.

We wish to thank Hao-Wen Xi, J. D. Gunton and J. Viñals for sharing the results of their simulations, and Yuchou Hu and R. Ecke for useful discussions. This research was supported by the Department of Energy through Grant DE-FG03-87ER13738. S. W. M. acknowledges support from The Natural Sciences and Engineering Research Council of Canada, and E. B. from the Deutsche Forschungsgemeinschaft.

REFERENCES

commas).

* Present address: Department of Physics and Erindale College, University of Toronto, 60 St. George St. Toronto, Ontario, Canada M5S 1A7.

† Present address: Laboratory of Atomic and Solid State Physics, Cornell University, Ithaca, New York 14853.

1. M. C. Cross and P. C. Hohenberg, *Rev. Mod. Phys.*, in print.
2. R. M. Clever and F. H. Busse, sets *J. Fluid Mech.* **65**, 625 (1974).
3. F.H. Busse and R.M. Clever, *J. Fluid Mech.* **91**, 319 (1979).
4. We first observed the chaotic state under non-Oberbeck-Boussinesq (non-OB) conditions. See Ref. [11] and S. W. Morris, E. Bodenschatz, D. S. Cannell and G. Ahlers, sets *Bull. Am. Phys. Soc.* **37**, 1734 (1992).
5. G. Ahlers and R. P. Behringer, sets *Phys. Rev. Lett.* **40**, 712 (1978).
6. E. D. Siggia and A. Zippelius, sets *Phys. Rev. Lett.* **47**, 835 (1981).
7. V. Croquette, P. Le Gal, A. Pocheau and R. Guglielmetti, sets *Europhys. Lett.* **1**, 393 (1986).
8. V. Croquette, sets *Contemp. Phys.* **30**, 153 (1989).
9. H. Xi, J. D. Gunton and J. Viñals, preprint.

10. E. Bodenschatz, J. R. de Bruyn, G. Ahlers and D. S. Cannell, sets *Phys. Rev. Lett.* **67**, 3078 (1991).
11. We determined the validity of the Oberbeck-Boussinesq (OB) approximation to the Navier-Stokes equations for our fluid by calculating the non-OB parameter \mathcal{P} defined by F. H. Busse, sets *J. Fluid Mech.* **30**, 625 (1967). \mathcal{P} varies approximately as $\mathcal{P}_c(1+p\epsilon)$. We found $\mathcal{P}_c = -0.7, -1.05, -2.1$ and $p = 1.1, 1.46, 1.79$ for pressures $P = 41.5, 32.7$ and 25.6 bar, respectively. It is important to note that non-OB effects scale as $6\mathcal{P}^2/R_c$, where $R_c = 1708$, so that they need not be important when \mathcal{P} is $\mathcal{O}(1)$. See Ref. [10]. The Prandtl numbers σ were 1.06, 0.96 and 0.86 for $P = 41.5, 32.7$ and 25.6 bar, respectively. Experimentally, we found that the chaotic state was qualitatively the same over this range.
12. V. Steinberg, G. Ahlers, and D.S. Cannell, sets *Phys. Script.* **32**, 534 (1985).
13. G. Ahlers, D. S. Cannell, and V. Steinberg, sets *Phys. Rev. Lett.* **54**, 1373, (1985).
14. M. S. Heutmaker and J. P. Gollub, sets *Phys. Rev. A* **35**, 242 (1987).
15. Very recently, M. Assenheimer and V. Steinberg (preprint, Feb. 17, 1993) reported spatio-temporally chaotic behavior of a many-target pattern, as well as a transition to a many-spiral state, near the critical point of SF_6 .
16. M. A. Dominguez-Lerma, G. Ahlers and D. S. Cannell, sets *Phys. Fluids* **27**, 856 (1984).
17. G. Ahlers, D.S. Cannell, and M.A. Dominguez-Lerma, sets *Phys. Rev. Lett.* **27**, 1225 (1983).

18. A. Pocheau, V. Croquette and P. Le Gal, sets *Phys. Rev. Lett.* **55**, 1094 (1985).
19. V. Croquette, sets *Contemp. Phys.* **30**, 113 (1989).

FIGURE CAPTIONS

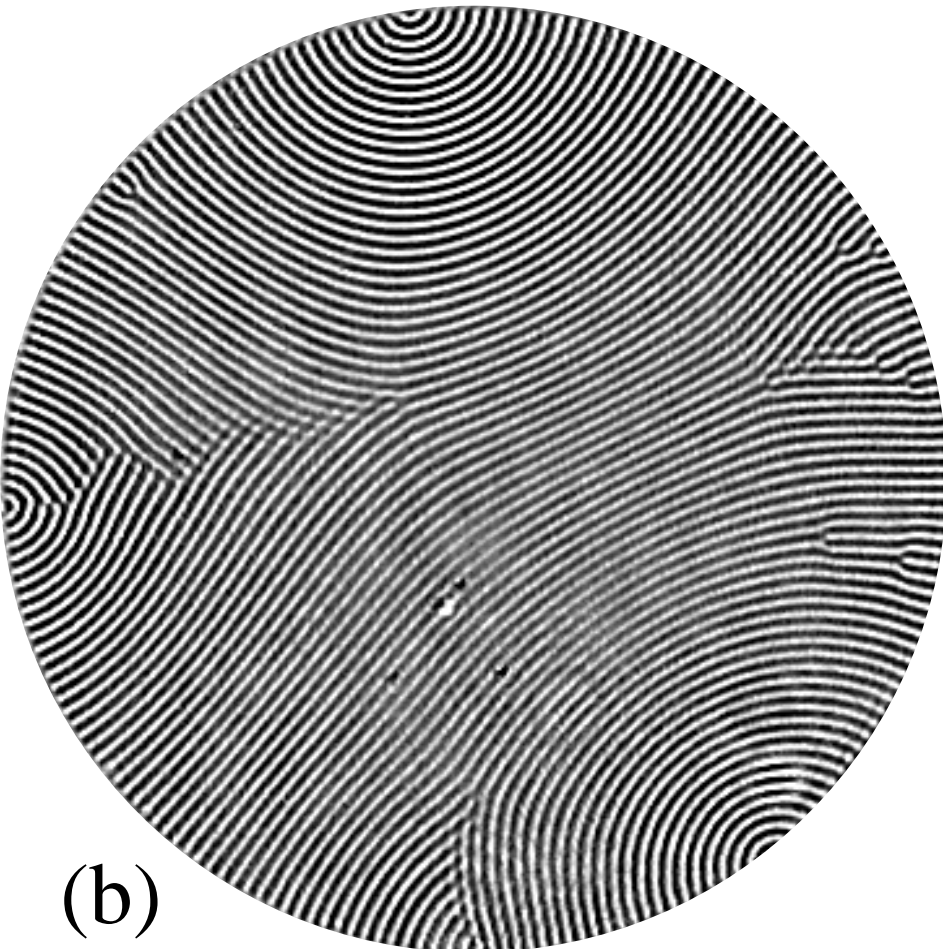
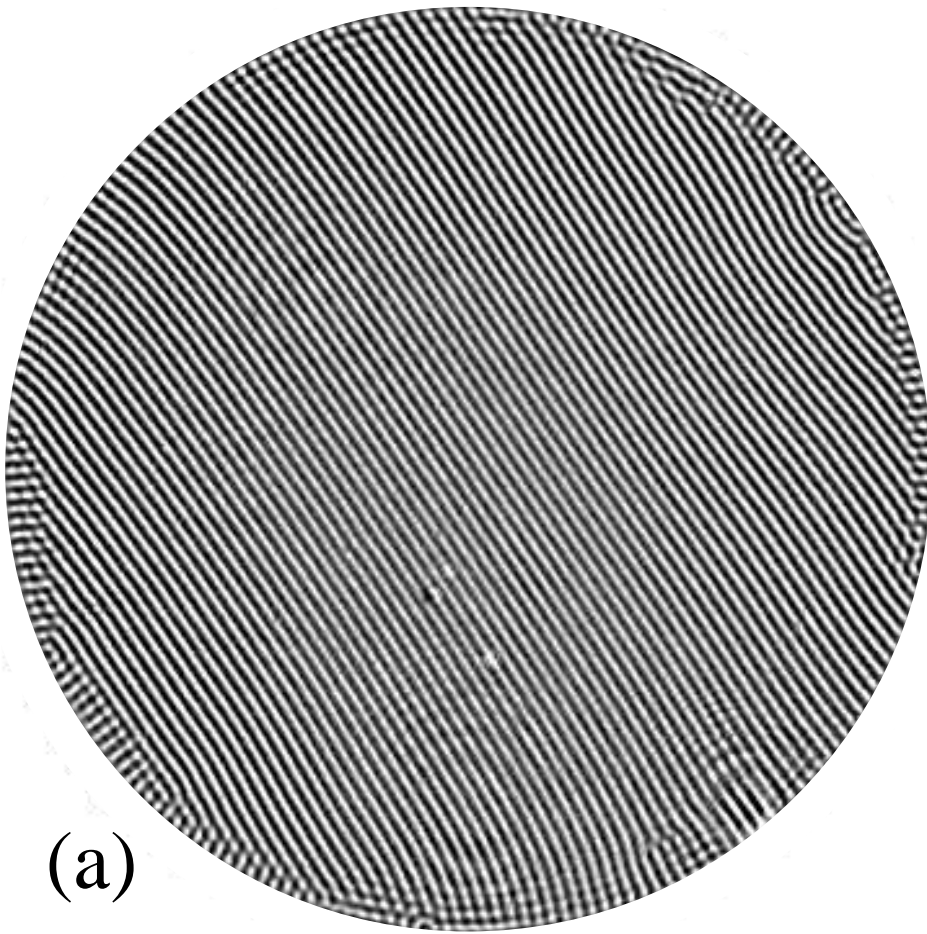
Fig. 1. Examples of patterns observed for $\epsilon \lesssim 0.2$. (a) $\epsilon = 0.040$, nearly perfect straight rolls. (b) $\epsilon = 0.116$, the global texture is dominated by curved rolls due to a few focus singularities on the sidewalls.

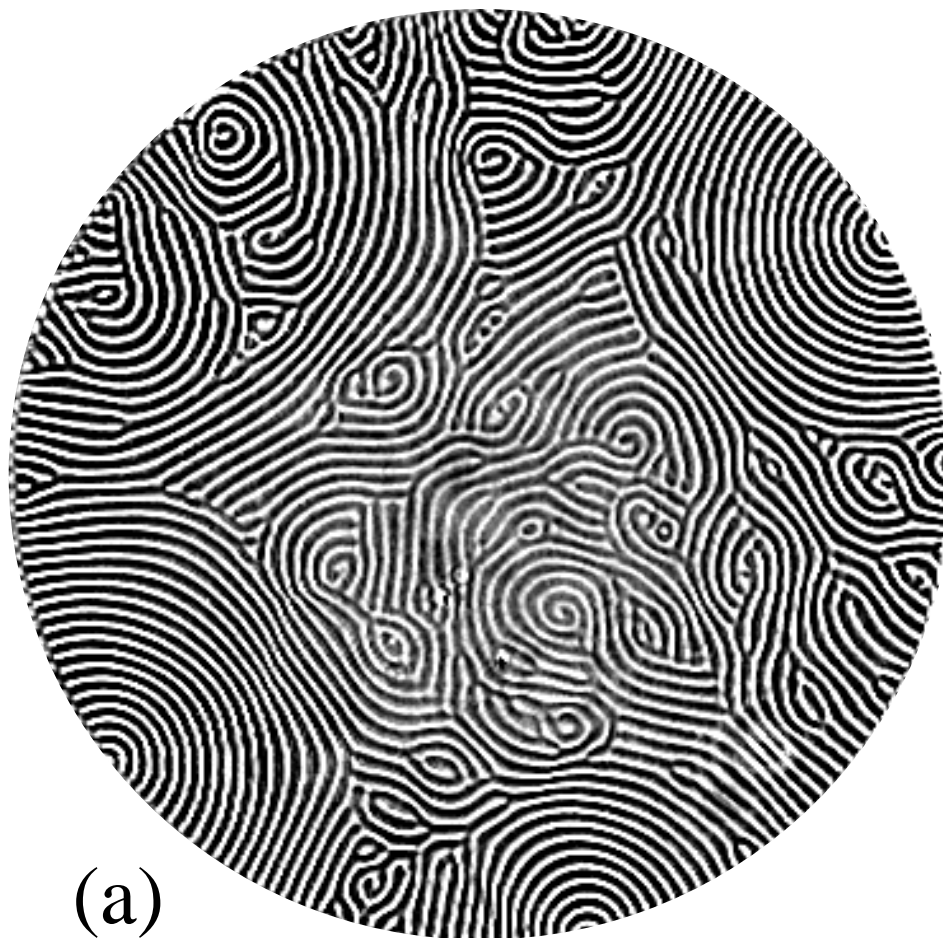
Fig. 2. Pattern sequence as ϵ is increased. (a) $\epsilon = 0.465$, coexistence of sidewall foci with a central chaotic region. (b) $\epsilon = 0.721$, spiral defect chaos completely fills the cell.

Fig. 3. The azimuthally and time averaged structure function of the pattern at $\epsilon = 0.465$. The dotted lines show the stability boundaries for straight rolls, from the Busse balloon.

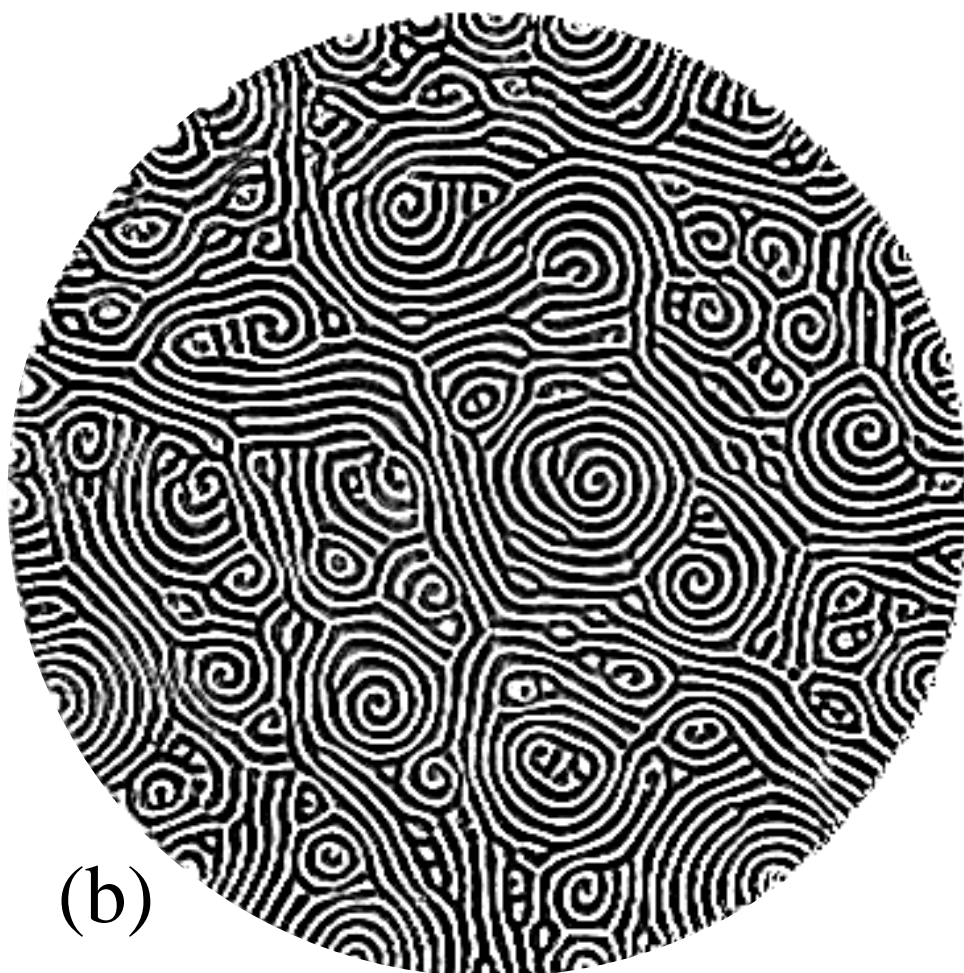
Fig. 4. The correlation length ξ vs. ϵ . The solid circles are for a pressure of 32.7 bar ($\mathcal{P}_c = -1.05, \sigma = 0.96$, see Ref. [11]), and the straight line is a fit to $\xi = \xi_0 \epsilon^{-\nu}$. The triangles and squares show ξ for 25.6 bar ($\mathcal{P}_c = -2.1, \sigma = 0.86$) and 41.5 bar ($\mathcal{P}_c = -0.7, \sigma = 1.06$), respectively.

Fig. 5. A comparison of $\langle k \rangle$ and width ξ^{-1} with the stability boundaries (the Busse balloon) predicted for straight rolls at $\sigma = 0.96$. The dashed curve is the neutral curve. The solid circles indicate $\langle k \rangle$, while the horizontal bars extend by $\pm \xi^{-1}$.





(a)



(b)

